

Evolution of the Fermi Surface across a Magnetic Order-Disorder Transition in the Two-Dimensional Kondo Lattice Model: A Dynamical Cluster Approach

L. C. Martin and F. F. Assaad¹

¹ *Institut für Theoretische Physik und Astrophysik,
Universität Würzburg, Am Hubland, D-97074 Würzburg, Germany*

We use the dynamical cluster approximation, with a quantum Monte Carlo cluster solver on clusters of up to 16 orbitals, to investigate the evolution of the Fermi surface across the magnetic order-disorder transition in the two-dimensional doped Kondo lattice model. In the paramagnetic phase we observe the generic hybridized heavy fermion band structure with large Luttinger volume. In the antiferromagnetic phase, the heavy fermion band drops below the Fermi surface giving way to hole pockets centered around $\mathbf{k} = (\pi/2, \pi/2)$ and equivalent points. In this phase Kondo screening does not break down but the topology of the resulting Fermi surface is that of a spin-density wave approximation in which the localized spins are frozen.

PACS numbers: 71.27.+a, 71.10.Fd, 73.22.Gk

In its simplest form, the Kondo lattice model (KLM) describes a lattice of spin 1/2 magnetic moments coupled antiferromagnetically via an exchange coupling J to a single band of conduction electrons and is believed to capture the physics of heavy fermion materials such as CeCu₆. The huge mass renormalization can be attributed to the coherent superposition of individual Kondo screening clouds and the resulting metallic state is characterized by a Fermi surface (FS) with Luttinger volume containing both conduction and localized electrons. At constant density, the J dependence of the inverse effective mass — or the coherence temperature — has been argued to track the single ion Kondo scale [1, 2]. Competing with Kondo screening, the localized spins interact indirectly via magnetic polarization of the conduction band. This RKKY scale dominates at low values of the exchange coupling and is the driving force for the observed magnetic order-disorder quantum phase transitions in those materials [3]. The nature of this phase transition is of current interest following experimental results suggesting a sudden change in the FS topology at the quantum critical point (QCP) for the heavy fermion metal YbRh₂Si₂ [4]. Driving this system from the non-magnetic heavy fermion metallic phase to the antiferromagnetic (AF) metallic phase causes a rapid change in the low temperature Hall coefficient which is extrapolated to a sudden jump at $T = 0$. Since the low-temperature Hall coefficient is related to the FS topology the results are interpreted as showing a sudden reordering of the FS at the QCP from a *large* FS, where the local moment impurity spins are included in the Luttinger volume, to a *small* FS where the impurity spins drop out of the FS volume. This scenario lies at odds with the Hertz-Millis description of the quantum phase transition [5, 6] and has triggered alternative descriptions [7, 8]. In this study it is exactly this issue which we investigate using the Kondo lattice as our

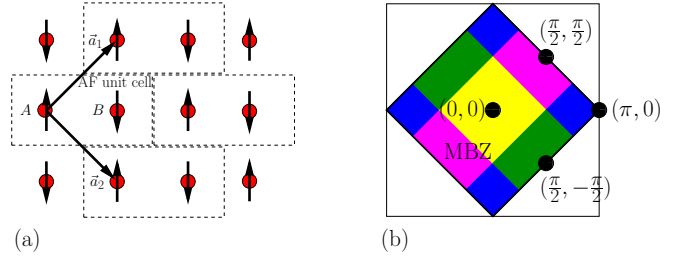


FIG. 1: (a) Definition of the real space basis vectors, unit cell and orbital indices (b) The reduced Brillouin zone and k-space patching for a cluster with $N_c^{AF} = 4$

model system:

$$H = \sum_{\mathbf{k}, \sigma} \epsilon(\mathbf{k}) c_{\mathbf{k}, \sigma}^\dagger c_{\mathbf{k}, \sigma} + J \sum_{\mathbf{i}} \mathbf{S}_{\mathbf{i}}^c \cdot \mathbf{S}_{\mathbf{i}}^f \quad (1)$$

with $c_{\mathbf{k}, \sigma}^\dagger$ creating a conduction electron on an extended orbital with wave vector \mathbf{k} and a z-component of spin $\sigma = \uparrow, \downarrow$. The spin 1/2 degrees of freedom, coupled via J , are represented with the aid of the Pauli spin matrices $\boldsymbol{\sigma}$ by $\mathbf{S}_{\mathbf{i}}^c = \frac{1}{2} \sum_{s, s'} c_{\mathbf{i}, s}^\dagger \boldsymbol{\sigma}_{s, s'} c_{\mathbf{i}, s'}$ or the equivalent definition for $\mathbf{S}_{\mathbf{i}}^f$ using the localized orbital creation operators $f_{\mathbf{i}, \sigma}^\dagger$. The KLM forbids charge fluctuations on the f -orbitals and as such the constraint of one electron per localized orbital must be included. To avoid particle-hole symmetry at half-band filling, we opt for a dispersion relation: $\epsilon(\mathbf{k}) = -2t[\cos(k_x) + \cos(k_y)] - 2t'[\cos(k_x + k_y) + \cos(k_x - k_y)]$ where t and t' are the first and second nearest neighbor hopping matrix elements respectively. We use $t'/t = -0.3$ throughout our calculations.

Method - To solve the above model, we apply the dynamical cluster approximation [9, 10] (DCA) with a Hirsch-Fye quantum Monte Carlo (QMC) algorithm as cluster solver. The DCA relies on a k -space coarse graining. The Brillouin zone is divided into N_c patches with center \mathbf{K} and the original \mathbf{k} -vectors are given by: $\mathbf{k} = \mathbf{K} + \tilde{\mathbf{k}}$. The DCA boils down to satisfying momen-

tum conservation only between patches. As can be seen within a skeleton expansion, this approximation yields a self-energy which is a functional of the coarsened-grained Green function: $\bar{G}(\mathbf{K}, i\omega_n) = \frac{N_c}{N} \sum_{\mathbf{k} \in \text{patch}} G(\mathbf{K} + \mathbf{k}, i\omega_n)$. With $G(\mathbf{k}, i\omega_n) = (G_0^{-1}(\mathbf{k}, i\omega_n) - \Sigma[\bar{G}(\mathbf{K}, i\omega_n)])^{-1}$ we obtain a self-consistent equation for \bar{G} . Each iteration step requires the solution of N_c impurities embedded in a fermionic bath given by: $\mathcal{G}_0^{-1} = \bar{G}^{-1} + \Sigma$.

Our particular implementation of the DCA allows for spontaneous antiferromagnetic symmetry breaking which enables us to not only localize the magnetic transition but also to carry out simulations within the magnetically ordered phase. The setup of our calculation is shown in Fig. 1a. Broken lattice symmetries are taken into consideration by defining a unit cell of two lattice sites containing, in total, two conduction electron orbitals and two localized f -electron orbitals. Within this unit cell, the up and down bath Green functions are allowed to take different values thus generating spin symmetry broken solutions. This is the smallest cluster, which we denote by $N_c^{AF} = 1$, with which we can capture AF ordering. Translational symmetry is now only assumed for the new basis vectors \mathbf{a}_1 and \mathbf{a}_2 giving the magnetic Brillouin zone (MBZ) in momentum space. DCA patching of the MBZ is demonstrated in Fig. 1b for a cluster of size $N_c^{AF} = 4$. Importantly, the DCA self-consistent equation for the lattice Green function becomes a 4×4 -matrix equation reflecting the four orbitals of the unit cell. In this study we use both $N_c^{AF} = 1$ and $N_c^{AF} = 4$ clusters. Although, for instance, with $N_c^{AF} = 1$ the coarse-grained self-energy has no momentum dependence a full \mathbf{k} -dependency of the lattice Green function enters via the non-interacting single-particle Green function $G_0(\mathbf{k}, i\omega_n)$, thereby allowing the calculation of a detailed FS regardless of the cluster size. Our implementation of the Hirsch-Fye impurity algorithm [11] to solve the cluster problem follows precisely the ideas introduced in Ref. [12].

Results - The DCA is justified if the underlying physics is driven by the frequency dependence of the self-energy as opposed to its momentum dependence. To check this we have carried out simulations at the particle-hole symmetric point ($t'/t = 0$ and $\langle n_c \rangle = 1$) and compared the results with the lattice QMC simulations of Ref. [12]. Although the DCA at $N_c^{AF} = 1$ grossly overestimates the coupling at which the magnetic order-disorder transition occurs, it reproduces the single particle spectral function both in the paramagnetic (PM) phase and, most importantly, in the AF phase remarkably well. This is demonstrated in Fig. 2 for the AF phase. Hence, the DCA is able to capture the delicate interplay between Kondo screening and magnetic ordering [12]. The sign problem which restricts finite sized lattice QMC studies of the KLM to the particle-hole symmetric case is not severe in the DCA approach close to half-filling and on cluster sizes up to 16 orbitals. Fig. 3 maps out the ground state

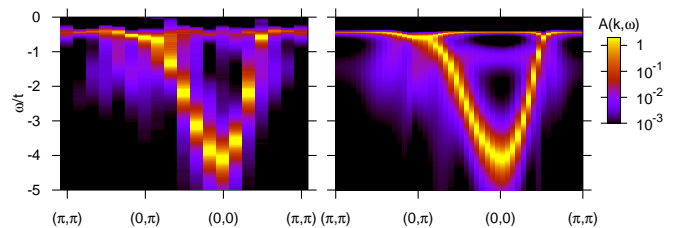


FIG. 2: (color online) Comparison of the single particle spectral function of the KLM at half-filling ($t'/t = 0$ and $\langle n_c \rangle = 1$) and with coupling $J/t = 1.2$ from (left) 12×12 -lattice QMC results as obtained with the projective auxiliary field algorithm of Ref. [12] and (right) DCA results with cluster size $N_c^{AF} = 1$ and $\beta t = 40.0$

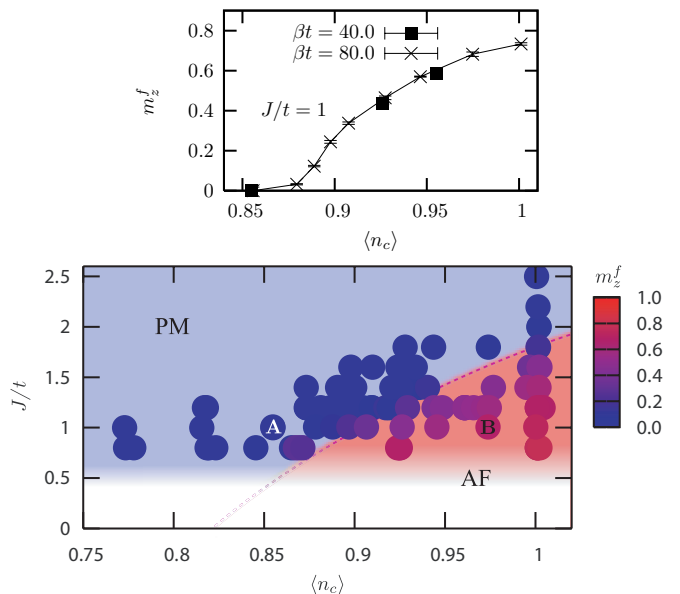


FIG. 3: (color online) Bottom: Magnetic phase diagram of the hole-doped KLM showing simulation results for the staggered magnetization m_z^f (color-coded circles) as a function of coupling J/t and conduction electron occupancy $\langle n_c \rangle$. Shading of AF and PM regions is a guide to the eye. Here $t'/t = -0.3$ and the calculations are carried out with the $N_c^{AF} = 1$ cluster. Top: m_z^f as a function of $\langle n_c \rangle$ at constant coupling $J/t = 1$

magnetic phase diagram of the KLM as a function of coupling J/t and conduction band hole-doping. Here, we are interested in ground state properties, so the choice for the inverse temperature βt must be large enough to ensure we are below the smallest scale in the problem: the coherence scale and/or the RKKY scale. Since the coherence scale decays exponentially with J/t we are limited to values of $J/t \geq 0.8$. This restriction arises since the computational time required by the QMC cluster solver scales as $(\beta N_c^{AF})^3$ [11]. On general grounds, we expect the onset of magnetism at small values of J/t since in this region the RKKY scale set by $J^2 \chi(\mathbf{q}, \omega = 0)$ dominates over the Kondo scale, $T_K \sim e^{-t/J}$. Here, $\chi(\mathbf{q}, \omega = 0)$ corresponds

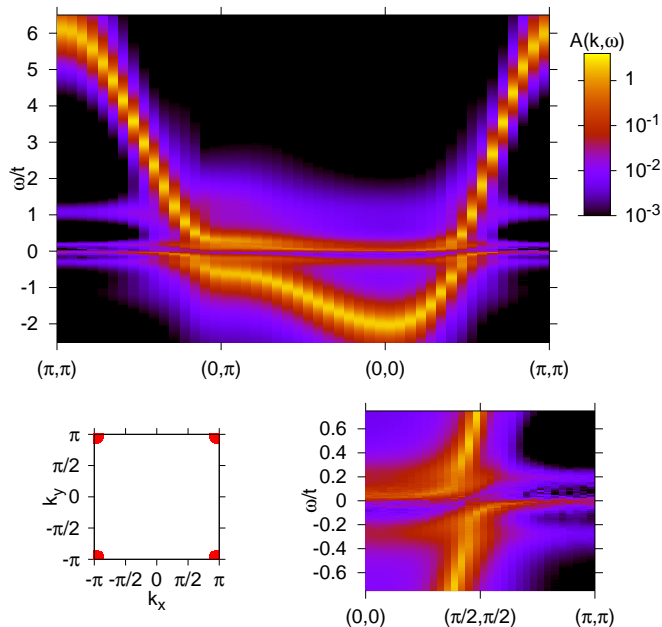


FIG. 4: (color online) DCA single particle spectrum for simulation A (see Fig. 3) in the PM region ($J/t = 1.0$, $\langle n_c \rangle = 0.855$ and $\beta t = 40.0$). The bottom right plot is a close-up of the main plot for energies around the Fermi-energy along the path $(0,0)$ to (π, π) . The bottom left plot shows the resultant Fermi-surface, plotted here via a large- N mean-field modeling of the DCA data (see text)

to the spin susceptibility of the conduction electrons. It is interesting to note that within the DCA approximation on cluster sizes up to $N_c^{AF} = 4$ the value of J/t at which antiferromagnetism sets in at half-band filling, $n_c = 1$, is only slightly affected by the choice of t'/t . On the other hand, the charge gap, which is known to scale with J/t in the particle-hole symmetric case ($t'/t = 0$) [12], is very much suppressed away from the particle-hole symmetric point. In particular, at $t'/t = -0.3$ our results are consistent with an exponential scaling of the charge gap [13]. Upon doping we observe a magnetic metallic state which as a function of decreasing coupling J/t progressively dominates the phase diagram. Finally, within our numerical accuracy, the staggered magnetization vanishes smoothly at the magnetic order-disorder transition thus lending support to a continuous transition (see Fig. 3, top panel).

Having established the magnetic phase diagram, we turn to our primary concern, namely the evolution of the FS across the magnetic order-disorder transition. Figs. 4 and 5 plot the single particle spectral function, $A(\mathbf{k}, \omega) = -\text{Im}G_{cc}^{ret}(\mathbf{k}, \omega)$ in the PM and AF metallic phases corresponding to the points A and B respectively in the phase diagram (Fig. 3). Analytic continuation to real frequencies was achieved with a stochastic analytic continuation method [14, 15].

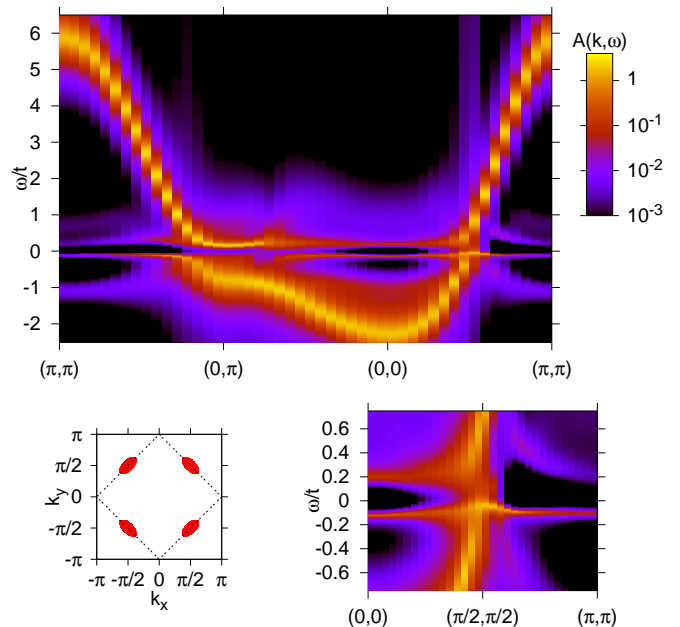


FIG. 5: (color online) DCA result for the single particle spectrum with $N_c^{AF} = 4$, $J/t = 1.0$, $\langle n_c \rangle = 0.977$ and $\beta t = 40.0$ in the AF region (point B in Fig. 3). The bottom right plot is a close-up of the main plot for energies around the Fermi-energy along the path $(0,0)$ to (π, π) . The bottom left plot shows the resultant Fermi-surface plotted here by fitting to the DCA spectrum using the mean-field form of Eq. 2.

The DCA spectral function in the PM phase (Fig. 4) is characterized by an extremely flat heavy fermion band crossing the FS in the vicinity of $\mathbf{k} = (\pi, \pi)$ and equivalent points. In the AF phase (Fig. 5), again at $J/t = 1.0$ but with $N_c^{AF} = 4$ and in close proximity to half-band filling the heavy fermion band centered around (π, π) is still present but has dropped below the Fermi energy and hole pockets centered around the wave vector $\mathbf{k} = (\pi/2, \pi/2)$ arise. This result is further supported by calculations at $J/t = 0.8$, $\beta t = 80$, closer to the magnetic transition ($n_c = 0.92$) but on smaller cluster sizes ($N_c^{AF} = 1$). The continued presence of heavy bands around (π, π) , although shifted to lower energies, indicates that partial Kondo screening still occurs in the magnetic phase. The main result of our spectral analysis however is the topological change of the FS when comparing the PM and AF phases.

Interpretation - As an aid to interpreting our DCA results we draw on the mean-field approximation of Zhang and Yu [16] which introduces the order parameters $\langle f_{i,\uparrow}^\dagger f_{i,\uparrow} - f_{i,\downarrow}^\dagger f_{i,\downarrow} \rangle = m_f e^{i\mathbf{Q}\mathbf{i}}$, $\langle c_{i,\uparrow}^\dagger c_{i,\uparrow} - c_{i,\downarrow}^\dagger c_{i,\downarrow} \rangle = -m_c e^{i\mathbf{Q}\mathbf{i}}$, with $\mathbf{Q} = (\pi, \pi)$, and $\langle f_{i,\uparrow}^\dagger c_{i,\uparrow} + c_{i,\downarrow}^\dagger f_{i,\downarrow} \rangle = \langle f_{i,\downarrow}^\dagger c_{i,\downarrow} + c_{i,\uparrow}^\dagger f_{i,\uparrow} \rangle = -V$. m_f and m_c are the staggered magnetizations of the impurity spins and conduction electrons respectively and V is a hybridization order parameter which mimics the screening of the impurity

spins. In this mean-field approach, which we stress is used here purely as a tool to aid interpretation of our DCA results, the constraint of unit occupation on the localized f -electron orbital is taken into account only on average by means of a Lagrange multiplier λ , as opposed to the exact single occupancy enforced within the DCA-QMC cluster solver.

The mean-field Hamiltonian, given by

$$\tilde{H} = \sum_{\mathbf{k} \in MBZ\sigma} \begin{pmatrix} c_{\mathbf{k}\sigma}^\dagger & c_{\mathbf{k}+\mathbf{Q}\sigma}^\dagger & f_{\mathbf{k}\sigma}^\dagger & f_{\mathbf{k}+\mathbf{Q}\sigma}^\dagger \end{pmatrix} \times \quad (2)$$

$$\begin{pmatrix} \epsilon_{\mathbf{k}} - \mu & \frac{Jm_f\sigma}{4} & \frac{JV}{2} & 0 \\ \frac{Jm_f\sigma}{4} & \epsilon_{\mathbf{k}+\mathbf{Q}} - \mu & 0 & \frac{JV}{2} \\ \frac{JV}{2} & 0 & \lambda & -\frac{Jm_c\sigma}{4} \\ 0 & \frac{JV}{2} & -\frac{Jm_c\sigma}{4} & \lambda \end{pmatrix} \begin{pmatrix} c_{\mathbf{k}\sigma} \\ c_{\mathbf{k}+\mathbf{Q}\sigma} \\ f_{\mathbf{k}\sigma} \\ f_{\mathbf{k}+\mathbf{Q}\sigma} \end{pmatrix}$$

results in a four-band energy dispersion relation, $E_n(\mathbf{k})$, in the MBZ.

The low temperature features of the PM phase are well understood in this mean-field framework by setting $m_f = m_c = 0$ in Eq. (2) which recovers the generic hybridized band structure of the large- N approximation, $E_{\pm}(\mathbf{k}) = \frac{\epsilon_{\mathbf{k}} - \mu + \lambda}{2} \pm \frac{1}{2} \left((\epsilon_{\mathbf{k}} - \mu - \lambda)^2 + (JV)^2 \right)^{\frac{1}{2}}$ with heavy bands crossing the Fermi energy in the vicinity of $\mathbf{k} = (\pi, \pi)$ and equivalent points in excellent agreement with the DCA result. In this mean-field modelling of the PM phase the Luttinger volume is given by $V_L^{PM}/V_{BZ} = (n_f + n_c)/2$, counting both conduction band electrons and impurity spins. Since the mean-field model accounts very well for the DCA spectral function in the PM phase, with the exception of the spectral weight around $\mathbf{k} = (0, 0)$ and $\omega/t \simeq -1/4$ [18], we attribute the DCA result with this same *large* Luttinger volume.

In the AF phase the DCA spectrum can again be well accounted for with the mean-field Hamiltonian of Eq. (2) but now setting non-vanishing staggered magnetizations, equal to the QMC measured observables, and using a non-zero hybridization value of $V = 0.3$ as fit parameter. In this fit, one band drops completely below the Fermi energy which itself is crossed only by the second band $E_2(\mathbf{k})$ in the vicinity of $\mathbf{k} = (\pi/2, \pi/2)$. In this case the Luttinger volume is given by $V_L^{AF}/V_{MBZ} = n_c$ and the topology of the FS is that of a spin-density wave approximation ($V = 0, m_f = 1, m_c \neq 0$ in Eq. (2)) where the f -electrons are frozen and do not participate in the Luttinger sum rule. Hence, we coin the FS, obtained from the DCA spectrum, as *small*.

We note that similar results have recently been observed in a variational Monte-Carlo approach to the KLM [17]. A major difference however is that the magnetic phase transition separating topologically different Fermi surfaces is of first order in the variational approach [17]. In contrast, the DCA calculation presented here supports a continuous transition in accordance with experimental findings.

Conclusions - We have presented large scale DCA calculations of the Kondo lattice model, and mapped out the magnetic phase diagram in the J/t versus doping plane. We have tested the approximation and seen remarkable agreement with lattice QMC methods with respect to the single particle spectral function. In particular, the approximation captures the delicate interplay between Kondo screening and magnetic ordering. Across the magnetic phase transition, the data shows a change in the topology of the FS from a large FS in the PM state to a small FS with hole-pockets centered around $\mathbf{k} = (\pi/2, \pi/2)$ in the AF phase. This change in topology of the FS is not linked to the breakdown of Kondo screening, and is consistent with a jump in the Hall coefficient as observed experimentally [4]. This jump in the Hall coefficient is not linked to a first order transition since within our numerical accuracy the staggered magnetization is a continuous function of the control parameter driving the quantum phase transition.

We would like to thank the Forschungszentrum Jülich for generous allocation of CPU time on the IBM Blue Gene/L and the DFG for financial support. We thank K. Beach, S. Capponi, S. Hochkeppel, T. C. Lang, T. Pruschke and M. Vojta for conversations.

-
- [1] S. Burdin, A. Georges, and D. R. Grempel, Phys. Rev. Lett. **85**, 1048 (2000).
 - [2] F. F. Assaad, Phys. Rev. B **70**, 020402(R) (2004).
 - [3] S. Doniach, Physica B **91**, 231, (1977).
 - [4] S. Paschen, T. Lühmann, S. Wirth, P. Gegenwart, O. Trovarelli, C. Geibel, F. Steglich, P. Coleman, and Q. Si, Nature **432**, 881 (2004).
 - [5] J. A. Hertz, Phys. Rev. B **14**, 1165 (1976).
 - [6] A. J. Millis, Phys. Rev. B **48**, 7183 (1993).
 - [7] Q. Si, S. Rabello, K. Ingersent, and J. Smith, Nature **413**, 804 (2001).
 - [8] T. Senthil, M. Vojta, and S. Sachdev, Physical Review B (Condensed Matter and Materials Physics) **69**, 035111 (2004).
 - [9] M. H. Hettler, M. Mukherjee, M. Jarrell, and H. R. Krishnamurthy, Phys. Rev. B **61**, 12739 (2000).
 - [10] T. Maier, M. Jarrell, T. Pruschke, and M. H. Hettler, Rev. Mod. Phys. **77**, 1027 (2005).
 - [11] J. E. Hirsch and R. M. Fye, Phys. Rev. Lett. **56**, 2521 (1986).
 - [12] S. Capponi and F. F. Assaad, Phs. Rev. B **63**, 155114 (2001).
 - [13] L. C. Martin and F. F. Assaad, to be published .
 - [14] A. W. Sandvik, Phys. Rev. B **57**, 10287 (1998).
 - [15] K. S. D. Beach, cond-mat/0403055 (2004).
 - [16] G.-M. Zhang and L. Yu, Phys. Rev. B **62**, 76 (2000).
 - [17] H. Watanabe and M. Ogata, Physical Review Letters **99**, 136401 (2007).
 - [18] We note that this feature is present both in the DCA on clusters up to 16 orbitals as well as in the DMFT approach. Hence, it cannot originate from magnetic fluctuations. A detailed understanding of this feature is

presently under investigation